The relation of moist symmetric instability and upper-level potential-vorticity anomalies to the observed evolution of cloud heads

By R. S. DIXON[1]*, K. A. BROWNING[1] and G. J. SHUTTS[2]
[1]*University of Reading, UK*
[2]*Met Office, UK*

SUMMARY

The cloud-head phenomenon has been known for some time as a precursor of rapid cyclogenesis. Based upon satellite imagery, two stages of cloud-head development are identified in this study that can be related to early and late stages of the associated cyclone. Weakly convex cloud heads emerge from the baroclinic zone at an early stage in cyclogenesis and strongly convex cloud heads develop in association with the rapid deepening of the cyclone. Trajectories are used to highlight the role of an upper-level potential-vorticity (PV) anomaly in the growth of the strongly convex cloud head and the main flow associated with the growth of the strongly convex cloud head is viewed using isentropic analysis. The possible role of moist symmetric instability in the development of both weakly and strongly convex cloud heads is discussed and a new diagnostic for measuring the vertically integrated extent of realizable symmetric (VRS) instability, based on the moist geostrophic PV, is introduced.

KEYWORDS: Extratropical cyclones   Rapid cyclogenesis   Satellite imagery

1. INTRODUCTION

The cloud-head phenomenon has been known for some time as a harbinger of extratropical cyclones with strong winds. The term 'cloud head' was first used by Böttger *et al.* (1975), who identified such a cloud feature in satellite imagery as a precursor to the development of storms over the Atlantic which were often accompanied by winds of hurricane force. Since then, the cloud-head phenomenon has been noted on a number of occasions, and studied in some cases in more detail (e.g. Young *et al.* 1987; Shutts 1990a; Browning and Roberts 1994). Awareness of its importance grew following its identification in the 'October storm' of 1987 (Monk and Bader 1988) and it is recognized as an early warning of potentially rapidly deepening lows accompanied by damaging winds (McCallum and Norris 1990).

As an introduction to the cloud-head phenomenon, Figs. 1 and 2 summarize the structure of a typical mature cloud head that crossed the United Kingdom on 28 April 1992 as shown by mesoscale observations from a Doppler radar. This cloud head was associated with the cyclone observed during the FRONTS-92 experiment by Browning *et al.* (1997). Figure 1 shows the surface frontal analysis, taken from Fig. 4(b) of Browning *et al.* (1997), and the rainfall area and cloud-top height obtained from model output, radar network data and satellite imagery. The outer edge of the cloud head is shown in the top-left corner of the figure. The polar-front cloud band from which the cloud head emerges is shown over France. The precipitating region within the cloud head was scanned by the Doppler radar at Chilbolton to give the cross-section in Fig. 2, the position of which is shown in Fig. 1. The section is approximately normal to the orientation of the frontal zone at mid levels, extending north-westwards to the north of the bent-back warm front (Shapiro and Keyser 1990). The Doppler velocities in Fig. 2 provide an indication of the cross-frontal flow. The velocities of this frontal circulation are up to 6 m s^{-1} relative to the front in both branches of the frontal circulation. Air in the shaded region ascends in a slantwise manner from right to left, the cloud tops
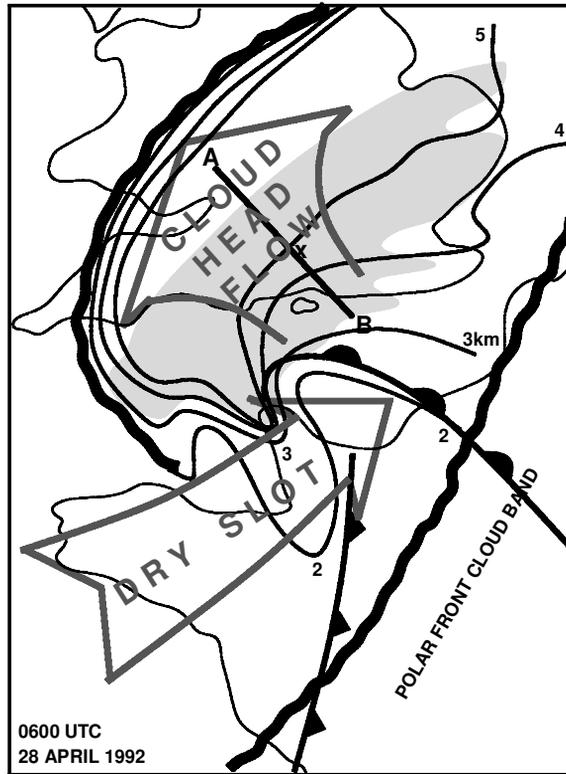
Figure 1.   Synthesis of the synoptic features at 0600 UTC on 28 April 1992. Thick wavy lines show the edges of the cloud shields associated with the polar-front cloud band and cloud head. Surface fronts are shown and the numbered lines in the cloud-head region depict the cloud-top height in kilometres derived from Meteosat imagery. Shading indicates the region of rainfall detected by the UK weather radar network. AXB indicates the position of the cross-section shown in Fig. 2; X is the position of the Chilbolton Doppler radar.

associated with this flow rising from 3 to 6 km. The region of ascent is undercut by air descending from left to right. The lack of radar echoes in the bottom left of the plot in this flow is due to the evaporation of falling precipitation. The evaporation is caused by the incursion of dry air towards the cyclone centre.

The atmospheric response to frontogenesis has been shown to be dependent on the moist symmetric stability of the atmosphere (Eliassen and Kleinschmidt 1957; Emanuel 1985; Thorpe and Emanuel 1985; Schultz and Schumacher 1999). Several case-studies of frontogenesis in the presence of weak symmetric stability or moist symmetric instability (MSI) (e.g. Moore and Blakley 1988; Lussky 1989; DeVoir 1998) have shown heavy rainfall organized in bands that are poorly resolved by numerical weather-prediction (NWP) models. Some studies (e.g. Shutts 1990a) have also mooted the possibility that MSI is involved in the development of cloud heads. Another factor that appears to affect cloud heads is the proximity of an upper-level potential-vorticity (PV) anomaly: cloud heads with strongly convex outer boundaries seem to occur in these circumstances.

The purpose of this paper is to use satellite imagery and NWP model analyses and forecasts to support qualitatively the hypotheses that:

• An upper-level potential-vorticity anomaly (tropopause depression) plays a role in causing a cloud head to become increasingly convex with time.
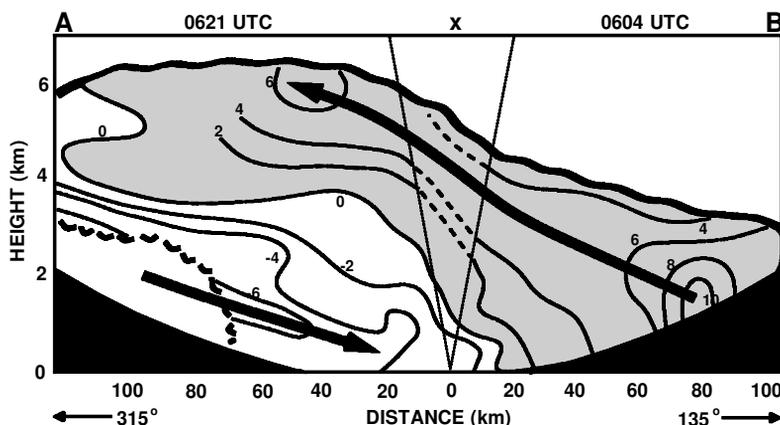
Figure 2.   Cross-section of Doppler velocity along AXB in Fig. 1 obtained with the Chilbolton Doppler radar through the mature cloud head that crossed England and Wales on 28 April 1992. The cross-section was obtained from a pair of scans, one towards 135° at 0604 UTC and the other towards 315° at 0621 UTC. Solid isopleths are radial (i.e. nearly horizontal) velocity in m s^{-1}, positive values and shading indicating front-relative flow from right to left and unshaded regions left to right. Dashed isopleths between the two thin lines directed upwards from the origin, and black areas at low elevation angles, indicate regions missing from the radar scans. Bold arrows, indicating slantwise ascent and descent, were inferred qualitatively from the pattern of horizontal flow. The thick black wavy line indicates the cloud top as shown in Fig. 1, and the broken thick black cusped line in the lower-left portion of the figure indicates the base of radar-detectable precipitation.

● MSI can play a role in the initial formation of a cloud head, at which stage its outer edge is often weakly convex. MSI may play a continuing role in the subsequent evolution of a cloud head.

The diagnostics shown in the paper are derived from the limited-area (LAM) version of the Met Office's Unified Model (Cullen 1993). The LAM was used operationally until the start of 1998 and its domain covers Europe, the North Atlantic and the eastern seaboard of the USA. It has a rotated latitude/longitude coordinate system with a pole at 160°E, 30°N, which ensures even grid spacings as the equator of the rotated grid passes roughly through the centre of the domain. Grid spacings are every 0.4425 degrees in latitude and longitude and close to 50 km over much of the domain. The model has 19 vertical levels, based upon hybrid pressure coordinates. These follow the terrain low down and are on pressure levels near the top of the domain, with a compromise in between. Vertical grid spacings are between 50 m in the boundary layer to over 2 km in the stratosphere, with mid-tropospheric spacings typically 500 m to 1 km. Boundary conditions for the LAM are taken from global-model forecasts from earlier runs.

Section 2 provides a short review of cloud-head structure and proposes a simple naming scheme that is used within the paper. Section 2 continues by showing qualitatively the role of upper-level PV anomalies in the evolution of the mature cloud head, using isentropic and trajectory analyses. Section 3 then looks at MSI and its likely relevance to the development of cloud heads in both their early and mature stages of development. Also, a selection of synoptic situations that bore cloud heads is described, using a new diagnostic that highlights regions where, according to the model, the atmosphere is moist symmetrically unstable. A schematic model of a developing cloud-head system is shown as a means of concluding the paper.

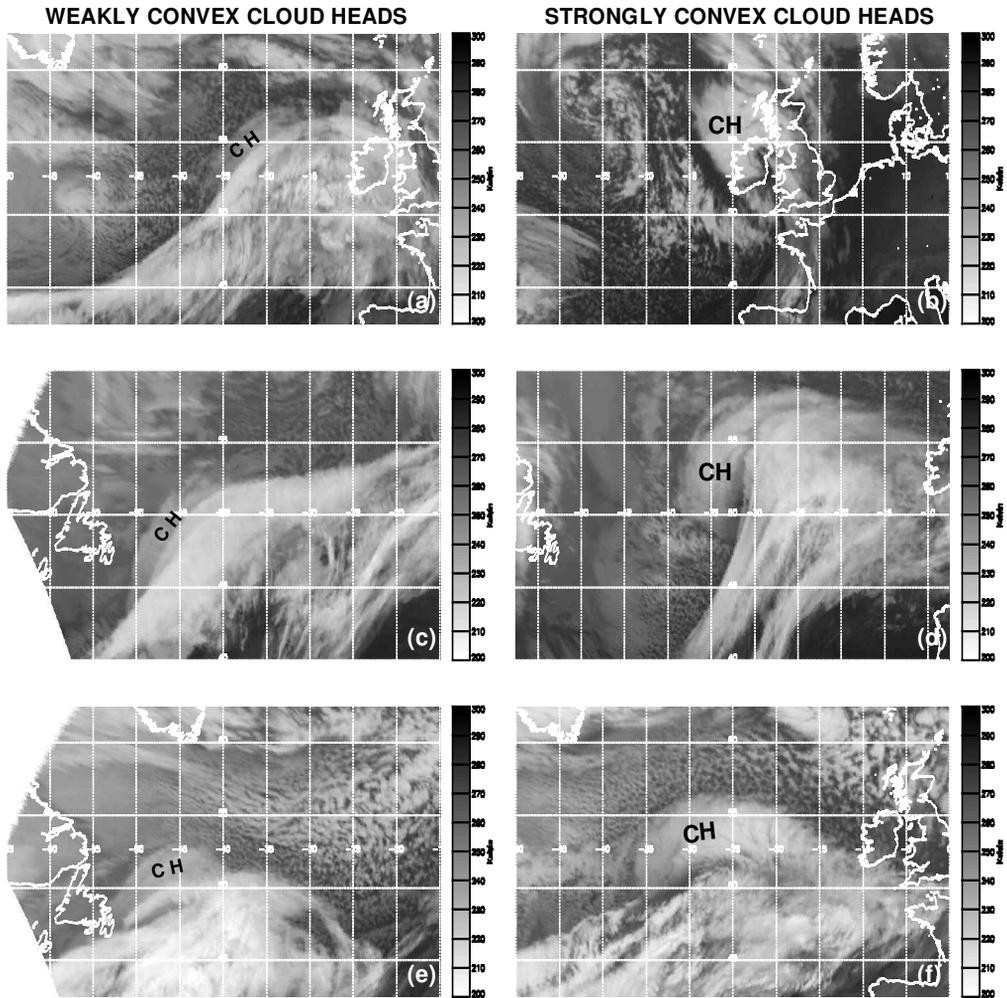**WEAKLY CONVEX CLOUD HEADS**   **STRONGLY CONVEX CLOUD HEADS**

Figure 3.   Meteosat infrared imagery showing cloud heads (CH) at both the weakly and strongly convex stages. Weakly convex cloud heads are shown in (a), (c) and (e) and correspond to 0600 UTC on 17 February 1997, 0130 UTC on 26 March 1998 and 0700 UTC on 25 December 1998, respectively. Strongly convex cloud heads are shown in (b), (d) and (f) and correspond to 1800 UTC on 24 October 1995, 1930 UTC on 26 March 1998 and 2000 UTC on 25 December 1998, respectively. The pair of images (c) and (d) correspond to different stages of the same system, as do images (e) and (f).

2.   THE EVOLVING STRUCTURE OF CLOUD HEADS

We first define a simple naming convention for cloud heads, based on an aspect of their structure that is indicative of their stage of development. Analysis of satellite imagery has suggested similarities in the shapes of emerging cloud heads as they develop. Initially the cloud head emerges from beneath the polar-front cloud band (PFCB) as a rather uniform sheet of cloud with a weakly convex outer edge; Figs. 3(a), (c) and (e) are satellite images showing such a development with a band of lower cloud tops corresponding to a **weakly convex cloud head** (CH$_W$) emerging from beneath the poleward boundary of the higher-topped PFCB. Analysis of model diagnostics in emerging cloud-head cases (e.g. Fig. 5.2.71 in Bader *et al.* 1995) points to rearward-sloping wet-bulb potential-temperature (θ_w) frontal surfaces that typify cold anafronts.

The later stages of cloud-head development are indicated by the hooking of the trailing end of the cloud head and its outer edge becoming generally much more convex—hence we use the term **strongly convex cloud head** (CH_S) for this feature. Examples of these are shown in Figs. 3(b), (d) and (f). The strongly curved shape of the cloud head will be addressed later with reference to the encroachment of upper-level PV anomalies above the low-level baroclinic zone. Our naming scheme is subjective but can be applied to many developing cloud heads. However, not all cloud heads develop beyond the CH_W stage, and some cloud heads grow directly into a CH_S without the initial development of the CH_W. Whilst most cloud heads emerge from beneath a PFCB, some cloud-head-like structures can develop separate from the PFCB, at some distance from the cold-air side of the PFCB (Bader *et al.* 1995, Ch. 5).

We now look at the progression from the weakly convex to strongly convex cloud head and its relation to the interaction of an upper-level PV anomaly with the low-level baroclinic system.

(*a*) *Cross-sectional analysis*

In this section we show results from a model forecast of a developing cloud head from a run starting at 0600 UTC on 23 December 1997. The case-study was chosen because of the striking nature of the observed and modelled cloud head, the intense circulation that is developed by the model and the fact that the cloud head developed far enough into the cold air so as not to be obscured by, or confused with, the PFCB. Although the forecast timing and location of the cloud head was poor, it produced a broadly realistic cloud head. The use of a single forecast run is preferable to using successive analyses for two reasons. Firstly, the model's analyses are produced only every six hours. As mentioned later, this is only marginally sufficient for accurate trajectory analysis. Secondly, a single forecast run, though inaccurate in our example, provides a more coherent continuum of data, whereas the analyses are corrected by new observational data which tend to break the continuity.

Fig. 4(a) shows the model's 'pseudo' infrared image at 0600 UTC as the cloud head was starting to form in the imagery. This pseudo infrared image was obtained by scanning from the top of the model's data downward until a level was reached where the model is close to saturation; at this point the temperature was read off, giving the model's perceived cloud-top temperature. At this time, actual satellite imagery (not shown) was indicating the development of a CH_W. The model's vertical-velocity field in (c) suggests modest velocities in the developing cloud-head region and the 950 mb θ_w contours show a local region of slightly stronger gradients, but at this time there is no sign of identifiable warm or cold fronts, nor does the model show any clear evidence of the developing cloud head in the pseudo imagery: it merely shows a broad region of cloud within which the cloud head later formed. The cross-section in (e), whose position is highlighted by the dashed line in (c), shows modest vertical velocities (approximately 10 cm s^{-1}) in the cloud-head region and also an upper-level PV anomaly (tropopause fold) which will be analysed later by the use of trajectories. Finally, the cross-section in (g) shows that the θ_w surfaces in the cloud-head region are initially oriented almost vertically, in contrast with their later pronounced tilt.

Twelve hours into the forecast, the same selection of plots, in Figs. 4(b), (d), (f) and (h), appear more dramatic. At this time there is a close correspondence between the structure in Figs. 4(b), (f) and (h) and that shown in Figs. 5.2.70 and 71 in Bader *et al.* (1995). The pseudo infrared image shows a cloud feature with a higher cloud top embedded within the general area of cloudiness, the western part of which later developed into a separate cloud head. The vertical velocity in the main cloud head at
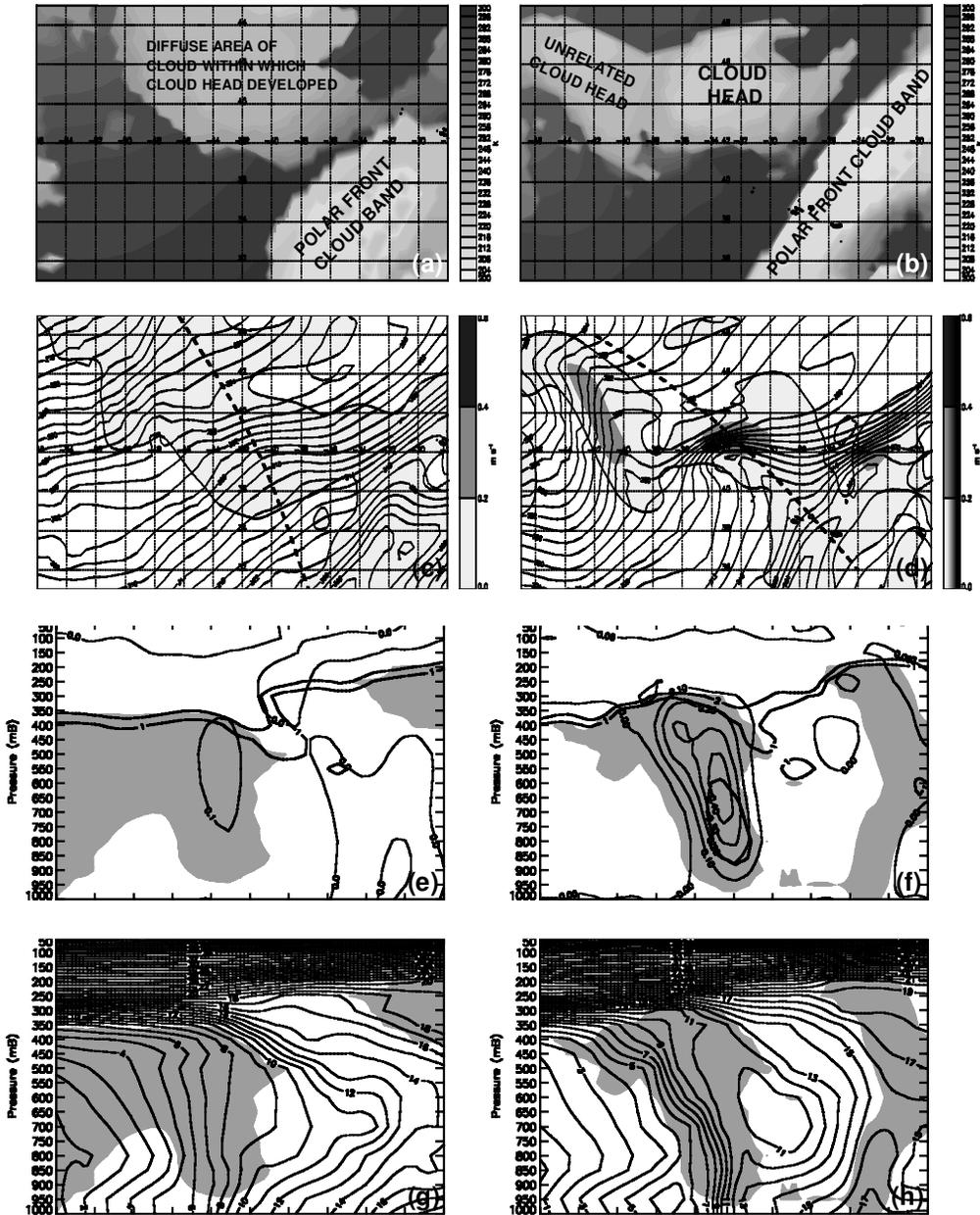
Figure 4. Unified Model diagnostics for the cloud head of 23 December 1997 taken from the 0600 UTC forecast run on this day: the analysis in the left column shows an early stage in the development of the cloud head and the T+12 forecast in the right-hand column shows the mature cloud head. Top two rows are plan views and bottom two rows are cross-sections along the dashed lines shown in (c) and (d). (a) and (b) pseudo infrared imagery (as defined in text), (c) and (d) contours of 950 mb wet-bulb potential temperature (θ_w, °C) with thick lines enclosing grey shades showing upward vertical velocity at 700 mb (0–0.2 m s^{-1} pale grey, 0.2–0.4 m s^{-1} medium grey, 0.4–0.6 m s^{-1} dark grey). (e) and (f) shaded regions show relative humidity >95%, thick contours 1 and 2 potential-vorticity units (after Hoskins *et al.* 1985) and thin contours the vertical velocity in 10 cm s^{-1} intervals. (g) and (h) shaded regions as in (e) and (f) but with contours of θ_w overlaid.

700 mb is much greater; maximum values are between 40 and 50 cm s^{-1}. Also notable is the lack of strong descent throughout the model cross-section; maximum values of descent are only 9 cm s^{-1}. The θ_w field also highlights an intense thermal gradient at the newly formed bent-back front that will be addressed later. The cross-section shown (the position of which is a compromise to cut through the vertical-velocity maximum, the strong thermal gradient of the bent-back front and the axis of the flow of high θ_w towards it) now reveals a more tilted structure to the θ_w surfaces. To the right of the cloud-head region in the cross-section, the θ_w field also shows a pronounced minimum associated with the dry intrusion, beneath which potential instability exists. In addition to the upper-level PV anomaly, a low-level PV anomaly can be seen which may have been generated through the release of latent heat. The zone of upward vertical velocities, like the θ_w isopleths, is tilted in the vertical and the maximum ascent appears in the mid troposphere between 700 and 500 mb. Comparison of precipitation rates between the two times shows an increase in the large-scale precipitation associated with the developing system from 1 mm h^{-1} at the earlier time to 7 mm h^{-1}.

The change in tilt of the θ_w surfaces in the cloud head between the times of the two cross-sections is part of a process that has been described by Browning *et al.* (1997) and Griffiths *et al.* (2000). The approach of an upper-level PV anomaly is associated with a circulation that decreases with distance beneath it. They show that the resulting differential rotation of the θ_w surfaces with height distorts these surfaces so as (a) to increase their rearward slope (i.e. cold-anafrontal structure) in the cloud-head region ahead of the PV anomaly and to the left of it (with respect to the direction towards which the PV anomaly is travelling), and (b) to produce forward-sloping θ_w surfaces (i.e. a cold-katafrontal structure with potential instability) in the dry-intrusion region behind and to the right of the PV anomaly.

(b) *Isentropic analysis*

Browning and Roberts (1994) used isentropic analysis on θ_w surfaces to depict the flows associated with the development of a strongly convex cloud head. The same approach was used to generate Fig. 5. Errors occur owing to the non-stationarity of the structure but the depiction of the broad pattern of flow is qualitatively valid. The time shown corresponds to the later of the two times in the previous plot, 12 hours into the 0600 UTC forecast run on 23 December 1997. The flows shown in Fig. 5 are system-relative winds on two different surfaces. The 295 K potential-temperature (θ) surface is used to represent the dry-intrusion air, and the 283.5 K θ_w surface is used to represent the main region of ascending motion associated with the cloud head. The thick line demarcates the cloud-head region, where the relative humidity is greater than 95% on this θ_w surface. The dry-intrusion air is seen to flow down the isentropic surface towards the cold front. One can also notice the fanning out of the dry-intrusion air behind the surface cold front. The flow in the cloud head (CH), is seen to ascend quite steeply from the surface up to approximately 8 km whereupon it accelerates to the north-east in an upper-level jet (outflow jet). Also evident is the anticyclonic curvature of the flow on this θ_w surface. Plots for the 281 K θ_w surface (not shown) depict the cold conveyor belt, a lower-level flow within the cloud head, ascending more gently than the overriding cloud-head flow shown in Fig. 5. Most of the precipitation is associated with the ascent of this air just to the north of the bent-back front. Along the bent-back front itself there is a band of convective precipitation: this is a favoured region for line convection. The main regions of ascent and descent, corresponding to the cloud-head and dry-intrusion flows,
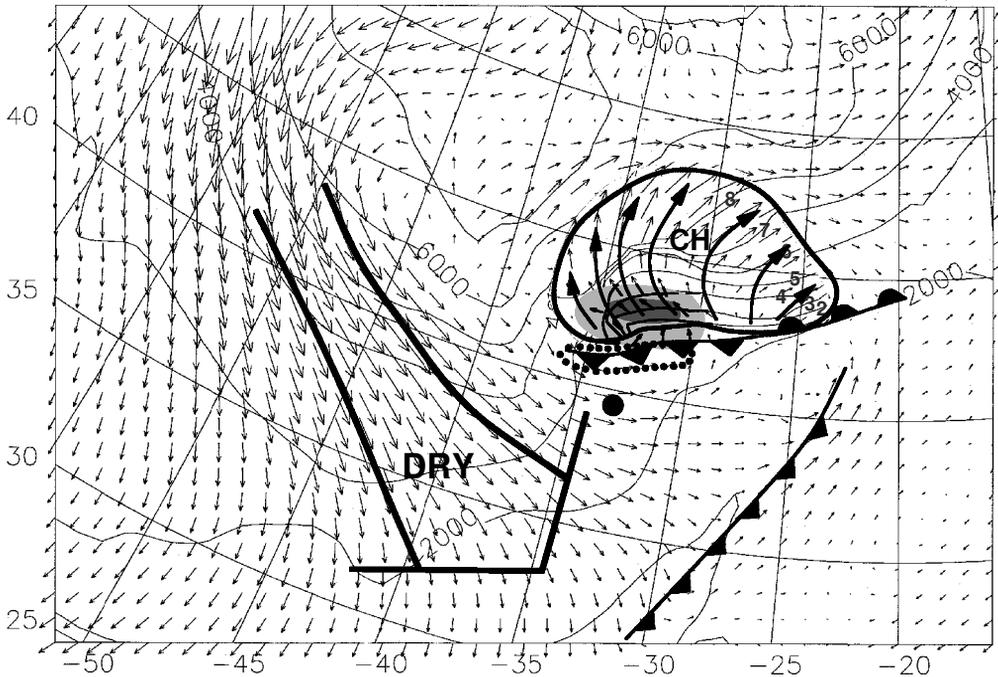
Figure 5. Cloud-head relative isentropic flows derived from the limited-area model at 1800 UTC from the 0600 UTC forecast (T+12) on 23 December 1997. Arrows within the thick contour in the region labelled CH mark the cloud-head flow on the 283.5 K wet-bulb potential-temperature (θ_w) surface. Numbers on the contours indicate the height of the surface in kilometres. Outside the cloud-head flow, the large arrow highlights the dry-intrusion flow on the 295 K potential-temperature (θ) surface with the heights of this surface shown in metres. The primary cold front, warm front and bent-back front are shown. The dotted line by the bent-back front shows the model's parametrized convective precipitation rate of 1 mm h^{-1}. The lightly shaded region shows large-scale rainfall rates greater than 2 mm h^{-1}, darker shading greater than 5 mm h^{-1}. The black dot shows the position of the potential-vorticity maximum at 500 mb which extended down from a 300 mb maximum located at 36°W, 42°N.

respectively, are seen to be located on opposite sides of the upper-level PV anomaly, the centre of which is represented in Fig. 5 by the large black dot.

(c) Trajectory analysis

Three-hourly model forecast data from the 0600 UTC run on the 23 December were used to perform a trajectory analysis of the developing system. The method used for calculating the trajectories is fully described in Wernli (1997). Wernli's method requires that a three-dimensional box be defined from which the trajectories of all parcels originally within this box are calculated. This provides a large number of trajectories and it is then possible to reduce the number of trajectories by applying selection criteria. A typical example might be to select all those trajectories that have ascended more than a prescribed height interval over the whole integration. Trajectories are picked from each model grid point in the horizontal and in 50 mb intervals in the vertical. Doty and Perkey (1993) performed sensitivity tests on frequency of wind data and its implications in the calculations of trajectories. Their findings suggested that six-hourly data are only marginally adequate for the most rapidly deepening cases. The cyclone in our study deepens rapidly in the forecast run, but the data interval is three hours, so
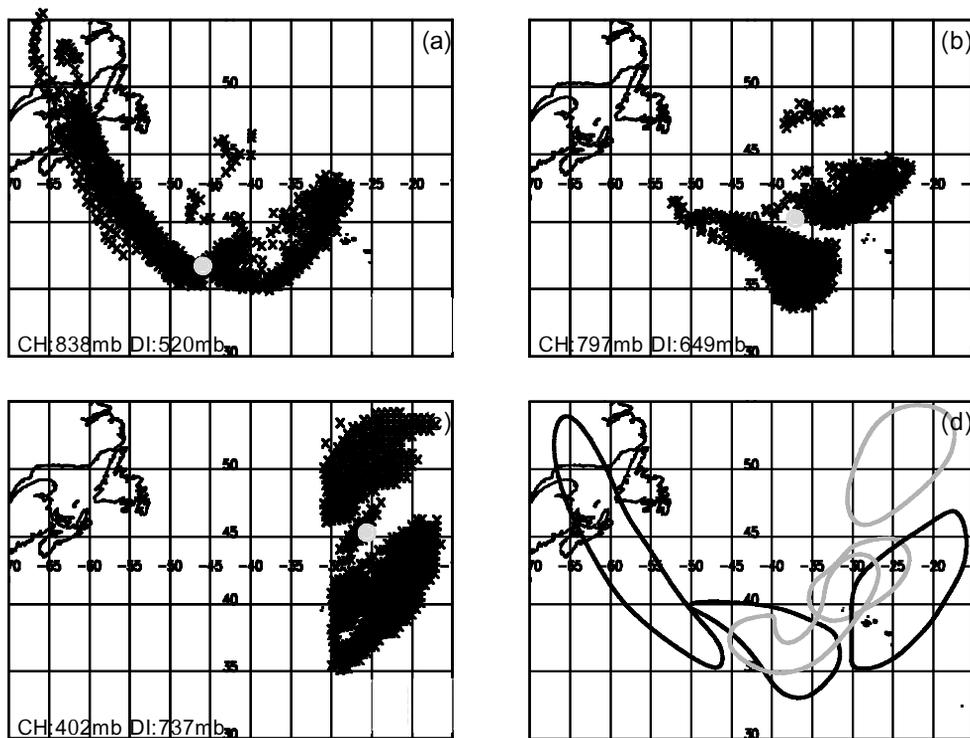
Figure 6. Positions of back trajectories of parcels at three times. Plots (a) to (c) show the descending dry intrusion and ascending cloud-head parcels at 0600 UTC, 1800 UTC on 23 December 1997 and 0600 UTC, 24 December 1997. Numbers in the bottom left of the initial plot show the average height of each set of parcels (CH = cloud head, DI = dry intrusion) at each time. Encircled grey dot shows the position of the upper-level potential-vorticity (PV) anomaly at 400 mb. Parcels associated with the DI are, respectively, to the west, south-west and south of this PV anomaly in (a), (b) and (c). Parcels associated with the CV are, respectively, to the east, north-east and north of the PV anomaly. Plot (d) shows the envelopes of all parcels in the CH and DI at times corresponding to (a), (b) and (c). Thick black envelopes surround the dry-intrusion parcels and grey envelopes surround the cloud-head parcels.

we are able to have some confidence in the trajectories. The Wernli routine allows us to perform both forward and backward trajectories but we shall present only the results of the backward trajectory calculations here. By placing a box around the model's dry intrusion as inferred from pseudo infrared imagery (not shown), backwards trajectories were run. An arbitrary value of relative humidity less than 60% is used to isolate the dry-intrusion parcels at T+24 and descent of more than 200 mb in the previous 24-hour period. In a similar way we have selected those trajectories that have ascended into the cloud head. Parcels in the cloud head were selected if their relative humidity at T+24 in the forecast run is greater than 95% and if they have ascended more than 300 mb at some point in the previous 24 hours.

The instantaneous positions of the ascending and descending parcels along the trajectories are shown at 12-hour intervals in Figs. 6(a), (b) and (c). It becomes clear from these plots that the cloud-head trajectories ascend ahead of the PV anomaly and the dry-intrusion trajectories descend behind and to the right of it (with respect to the direction towards which the PV anomaly is travelling). Closer inspection shows that the dry-intrusion air accomplishes more of its descent early in the lifetime shown. By the time the dry-intrusion air reaches the main low, it can begin to re-ascend, as noted
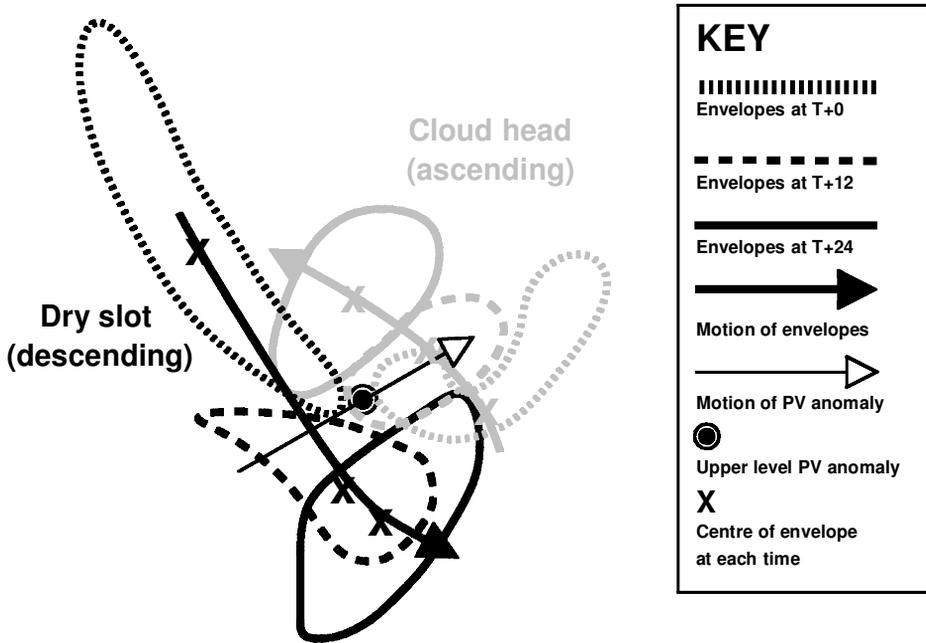
Figure 7. Envelopes of parcels relative to the moving upper-level potential-vorticity (PV) anomaly at 12-hour intervals from 0600 UTC on 23 December 1997. Grey shows the ascending parcels in the cloud head, black the descending parcels in the dry intrusion.

in previous work (Carr and Millard 1985). As noted above, potential instability can be created beneath the descending dry-intrusion air and its re-ascent can allow its release and lead to heavy convective precipitation.

These results are in line with the ideas of Hoskins *et al.* (1985) who show a pattern of descent behind a moving upper-level PV anomaly and ascent ahead of the anomaly. This point is made even clearer when we take the envelopes of the parcels shown in Figs. 6(a) to (c) and look at their motion *relative* to the moving PV anomaly, as shown in Fig. 7. The upper-level PV anomaly appears to be a pivot ahead of which the moist parcels ascend cyclonically within the strongly convex cloud head, and behind which the dry-intrusion parcels descend. The PV anomaly, when viewed in terms of the flows sketched in Fig. 1 can be seen to be associated with the production of both the strongly ascending cloud-head flow (sometimes referred to as a secondary warm conveyor belt, W2 (Bader *et al.* 1995, see their Fig. 5.2.70(b), p.273)) and the dry-intrusion flow where it enters the dry slot.

Cloud heads appear to have two distinct phases of growth. The CH_W first grows out from a low-level baroclinic zone, and often appears from beneath the PFCB. The satellite imagery shows a weakly convex-edged cloud distinguishable from the PFCB by its lower cloud tops (Figs. 3(a), (c) and (e)). The second stage of growth, corresponding to the development of the strongly convex cloud head, CH_S (Figs. 3(b), (d) and (f)), is associated with the encroachment of the upper-level PV anomaly on the baroclinic zone and often leads to the rapid development of the low-level cyclone system. The isentropic plots and trajectory plots show well the large-scale flows associated with upper-level PV anomalies that lead to the strongly convex cloud head. Ascent ahead of the upper-level PV anomaly lifts the air in the baroclinic zone cyclonically ahead of it

and this produces the strongly convex cloud head. The 'twisting' motion of the anomaly, in conjunction with any low-level vorticity, develops the low-level thermal field, leading to a redistribution of the thermal gradient and potentially explains the frontal fracture described by Shapiro and Keyser (1990). A key part of the frontal structure is the bent-back front. The model generates much higher vertical velocities and rainfall rates at its bent-back front than at the baroclinic zone associated with the CH_W.

We now look at the possible relevance of MSI in the development of frontal circulations associated with both weakly and strongly convex cloud heads.

3. POSSIBLE ROLE OF MOIST SYMMETRIC INSTABILITY IN THE DEVELOPMENT OF THE CLOUD HEAD

Moist symmetric instability is a manifestation of inertial instability that in atmospheric flows is usually made realizable by the effects of water phase changes in and near cloud systems. It is largely found where high vertical wind shears co-exist with strong horizontal thermal gradients and the atmosphere is weakly statically stable, for example in the vicinity of fronts. MSI may occur in frontal regions where the moist geostrophic PV, MPV_g, defined by

$$MPV_g = \frac{1}{\rho} \zeta_g . \nabla \theta_e \qquad (1)$$

(where ρ is the density; ζ_g is the geostrophic absolute vorticity vector and θ_e is the equivalent potential temperature) is negative. Detailed insight into MSI is provided in the early papers by Bennetts and Hoskins (1979) and Emanuel (1983). Often, it is supposed that MSI takes the form of a slantwise convecting plume that emerges from line convection at a cold anafront. In this situation, ascending air may be (weakly) moist convectively unstable at the line convection, but then, due to the quasi conservation of absolute momentum, releases kinetic energy in the form of a slantwise adjustment. In contrast to the cross-frontal circulations in a dry frontal zone, therefore, the ascending air in a moist symmetrically unstable environment takes the form of a shallow sloping sheet of strong vertical motion. Emanuel (1987) showed this to be true in the limit of very small (though positive) moist symmetric stability. Many examples exist in the literature of modelling and observational studies of frontal zones where regions of the atmosphere appear to be unstable or at least neutral to slantwise instability (see Schultz and Schumacher (1999) for a comprehensive bibliography).

(a) Example of a weakly convex cloud head and the associated moist symmetric instability

The rather straight-edged weakly convex cloud head that grows in the early stages of cyclone development is considered first. The example is taken from the Fronts and Atlantic Storm-Track EXperiment (FASTEX) Intensive Observing Period (IOP) 16. The cloud head emerged from the PFCB during the morning of 17 February 1997. Fig. 8(a) shows the satellite imagery at 0600 UTC on this day. CH marks the weakly convex cloud head emerging from beneath the PFCB. Alongside this, in (b), is an equivalent plot of the satellite imagery but using data from the LAM analysis. Comparing the two plots, it is clear that, although the model reproduces the poleward boundary of the PFCB rather well, the cloud head itself is not as well developed—if at all—in the LAM as in reality. Significantly, however, recent studies in the Joint Centre for Mesoscale Meteorology (Humphrey Lean, personal communication) show that the Unified Model is able to
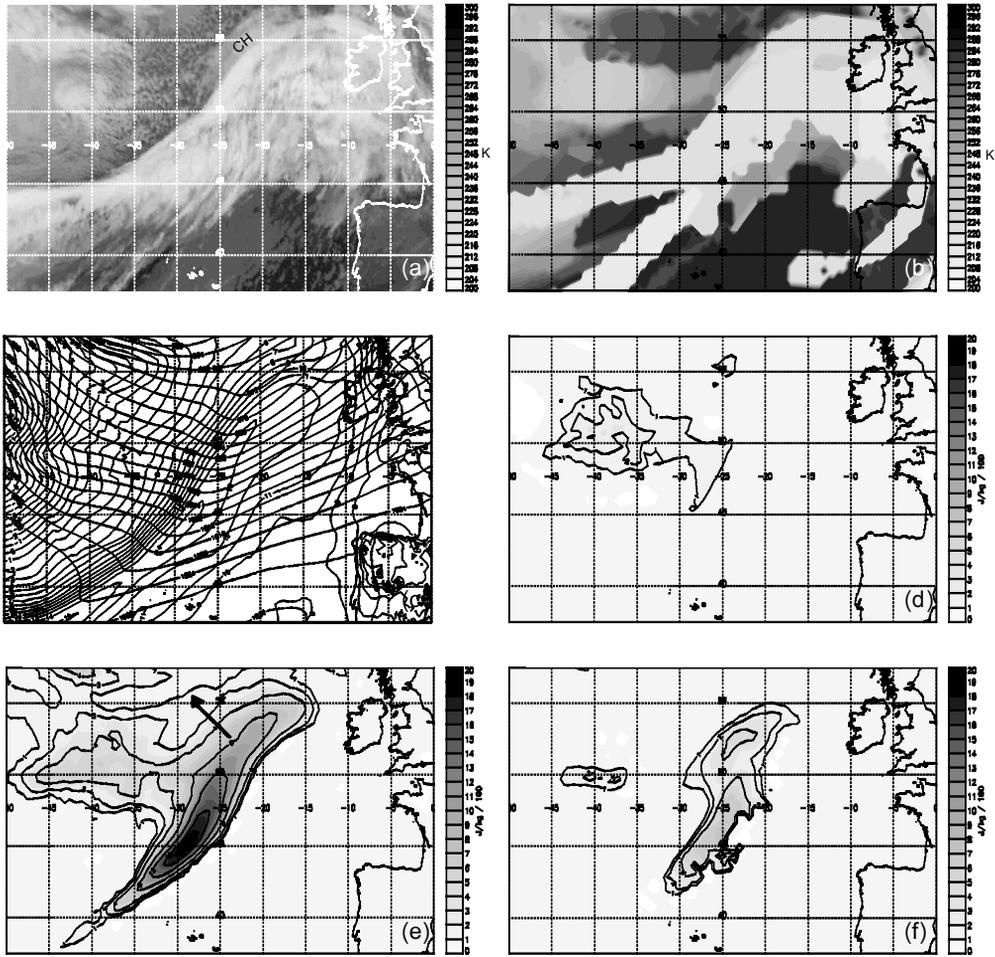
Figure 8. Satellite imagery and diagnostics for 17 February 1997 at 0600 UTC. (a) Meteosat infrared satellite imagery. CH marks the cloud head emerging to the north-west of a major polar-front cloud band. (b) Pseudo infrared imagery obtained from the limited-area model. (c) 950 mb wet-bulb potential temperature (°C, thin contours) and surface pressure (mb, thick contours). (d) Convective available potential energy (CAPE) calculated for parcels lifted from 950 mb. (e) Slantwise CAPE (SCAPE) calculated for parcels originating from 950 mb. (f) SCAPE calculated for parcels originating from 750 mb. The arrow in (e) is explained in the text. Contours of SCAPE and CAPE shown (in factors of 100 J kg^{-1}) are 1, 2, 4, 8, 12, 16, 20 and 25. White regions indicate negative values of SCAPE or CAPE.

reproduce the details of the cloud head at this stage when its grid spacing is reduced to 25 km or less. There is still not a closed low in the surface pressure analysis (Fig. 8(c)), although strong localized pressure falls are in progress in the region where the low is about to form.

Figure 8(d) shows the convective instability for parcels lifted from 950 mb, quantified by using the convective available potential energy (CAPE). There appears to be little CAPE in the region of the cloud head although there is a small region of CAPE up to approximately 300 J kg^{-1} in the cold air behind the developing system. For parcels lifted from 750 mb, the CAPE (not shown) is negligible everywhere.

Plots (e) and (f) show the slantwise CAPE (SCAPE). First calculated for model fields by Shutts (1990b), SCAPE is a measure of the potential for slantwise instability.

Shutts shows that measuring the profile of the atmosphere along the intersection of M and N surfaces, where M and N are the two components of the absolute momentum (given by $M = \int f \, dx + v$ and $N = \int f \, dy - u$), yields a quantitative estimate of the energy available to slantwise displacements. SCAPE and slantwise convection, respectively, are analogous to CAPE and vertical convection. Figure 8(e) shows that the SCAPE for parcels lifted from 950 mb is considerably greater than the corresponding CAPE, suggesting that energy is available to slantwise displacements despite there being very little energy available to vertical displacements. The direction of the release of CAPE through convection is upward. SCAPE, on the other hand, is calculated along M and N intersections and, in vertically sheared environments, these surfaces are inclined to the vertical. For this reason it is important to compare the orientation of the M and N intersection with that of the observed ageostrophic circulation. Therefore, also shown in Fig. 8(e) is an arrow representing the orientation of an M and N intersection in the vicinity of the cloud head: it can be seen that this points in the direction of the developing cloud head and thus SCAPE is potentially of relevance in this example. The component of absolute momentum normal to the arrow shown is assumed to be approximately conserved during slantwise ascent. Similar results apply at 750 mb (Fig. 8(f)) and, although less SCAPE is evident, there is still an appreciable amount. This suggests that the potential for MSI was present in depth in the region where the cloud head was emerging. The fact that the LAM did not generate a clear cloud head at this time may reflect its inability to resolve the release of MSI at this resolution (Persson and Warner 1993).

(b) *Example of a strongly convex cloud head and the associated moist symmetric instability*

The second example is from 25 December 1998. A cyclone with a pronounced cloud head crossed into the eastern Atlantic during the day. We will concentrate on the model analysis at 1800 UTC, when the cyclone was about to deepen rapidly and it possessed a strongly convex cloud head. Hand-drawn surface analyses from the Met Office show a dramatic deepening of this low of 23 mb in the 12 hours between 0000 and 1200 UTC on the following day. The plots in Figs. 9(a) and (b) show that the model was quite successful in producing the strongly convex cloud head (shown by CH), although it is slightly too far north. The system at this time shows the classical structure introduced by Shapiro and Keyser (1990) with a bent-back front and frontal fracture. Plot (d) shows very little CAPE accompanying the fronts at 950 mb; there was no CAPE at 750 mb. The SCAPE plots at 950 mb and 750 mb in (e) and (f), respectively, show a region of appreciable SCAPE (greater than 2500 J kg^{-1} for parcels lifted from 950 mb) at both levels. The location of the highest SCAPE at both levels is coincident with the bent-back front; other examples of bent-back fronts (not shown) always indicate very high (often greater than 2000 J kg^{-1}) SCAPE.

Also noteworthy is that the trailing cold-frontal region shows high levels of SCAPE. However, SCAPE along the cold front decreases close to the cyclone centre where the front is of the 'kata' variety. Several other examples showed the lack of SCAPE in cold katafronts and this suggests that the overrunning dry air acts to suppress the development of MSI. The overrunning air flow at mid levels is not parallel to the surface isotherms. The M and N intersections, unlike those in cold-anafrontal situations, bend in a manner that is not conducive to SCAPE, and moreover the flow in these situations is more likely to violate the two-dimensional assumption that underlies the theory of slantwise convection employed here.
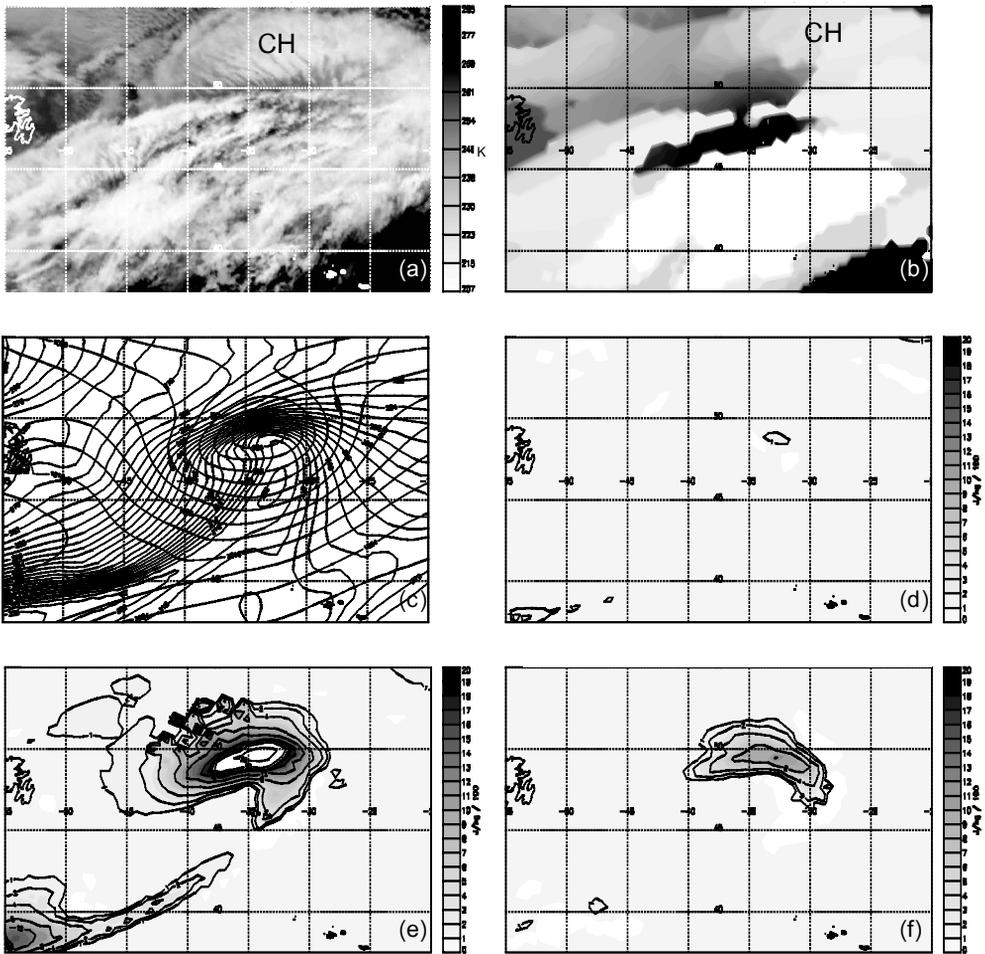
Figure 9. Satellite imagery and diagnostics from 25 December 1998 at 1800 UTC. (a) Infrared Meteosat imagery. (b) Pseudo-infrared imagery obtained from the limited-area model (same greyscale as (a)). (c) 950 mb wet-bulb potential temperature (K, thin contours) and sea-level pressure (mb, thick contours). (d) Convective available potential energy (CAPE) calculated for parcels originating from 950 mb. (e) Slantwise CAPE (SCAPE) from 950 mb. (f) SCAPE from 750 mb.

(c) Case-studies of other cloud heads using a new moist-symmetric-instability diagnostic

We now show a number of case-studies of cyclones that all possess cloud heads. For these examples, we introduce a new diagnostic based upon recommendations for MSI diagnostics made in the critical review of past MSI papers by Schultz and Schumacher (1999). The diagnostic we shall use provides a measure of the *Vertically integrated extent of Realizable Symmetric instability* and we shall refer to it as VRS. In contrast, any single SCAPE plot shows the potential for MSI for air originating at only one level and, therefore, does not give an indication of the full amount of MSI integrated vertically over all levels of origin.

The VRS diagnostic gives the extent of the regions in the model where the atmosphere has MSI that can be realized. Hoskins (1974) showed how in a dry, stably stratified atmosphere in thermal wind balance, when the geostrophic PV is less than zero,

the atmosphere is dry symmetrically unstable. The VRS diagnostic is based around the *moist* geostrophic PV, MPV_g, defined earlier. The VRS diagnostic measures the *number* of model layers (not necessarily contiguous) for which all of the following conditions are met:

- $MPV_g < 0$
- $\partial\theta_w/\partial p < 0$
- Relative humidity $> 95\%$
- Vertical velocity $(w) > 0$
- $\partial v_g/\partial x - \partial u_g/\partial y + f > 0$

where u_g and v_g are the u and v components of the geostrophic wind, respectively. Negative MPV_g indicates regions that are potentially symmetrically or convectively unstable, or a combination of the two; thus the second criterion is needed to eliminate any areas that might possess negative MPV_g owing to potential convective instability. Schultz and Schumacher (1999), referring to among others, papers by McNulty (1995) and Doswell III *et al.* (1996), stress the need for sufficient moisture and lift to be present before the instability can be realized. Thus, the moisture and lift requirements are given by the third and fourth criteria, respectively. The relative humidity is calculated with respect to ice for temperatures below $0\,^{\circ}$C and with respect to liquid for temperatures above this value. The fifth criterion refers to the absolute vorticity computed on an isobaric surface. Horizontal inertial instability, which can also lead to negative moist PV, is excluded by means of this criterion as it is deemed not to be a cloud-producing flow. The VRS diagnostic is the number of levels between 1000 and 100 mb at each grid point (the VRS diagnostic is computed at 50 mb intervals and thus there is a maximum of 19 levels) where the above criteria are met. Thus, the diagnostic illustrates the vertically integrated extent of the model that is unstable to MSI, though does not quantify the degree of moist symmetric instability in the same way that SCAPE purports to. The plots on the right-hand side of Figs. 10 and 11 show the VRS diagnostic for examples of weakly and strongly convex cloud heads, respectively; the chosen threshold for a significant region of MSI is three unstable levels. The position of the cloud head based upon the satellite imagery and model diagnostics for each case (not shown) is marked on each plot.

Clearly, in the weakly convex cloud head (CH_W) cases in Fig. 10, there is MSI along the main baroclinic zone close to the developing CH_W. Figure 10(e) shows an interesting double thermal structure in the developing FASTEX storm. A double cloud-head structure was obvious from satellite imagery at this time and this is mirrored in the VRS diagnostic in Fig. 10(f). Direct comparison can be made between Fig. 10(b) showing the VRS diagnostic for 0600 UTC on 17 February 1997 and the corresponding SCAPE plots in Figs. 8(e) and (f). The SCAPE plots suggest merely the *potential* for MSI. Comparison with the VRS diagnostic, showing where the model is diagnosing realizable instability, highlights that parts of the cloud-head region are *actually* sym-metrically unstable in depth. However, the trailing cold-frontal region, although clearly *potentially* symmetrically unstable as shown in the SCAPE diagnostic, has only a few levels that have realizable MSI according to the VRS diagnostic.

Three further examples in Fig. 11 show synoptic situations in which a strongly convex cloud head (CH_S) grew. The region of VRS in all the examples is split into two regions; one along the trailing cold front which has fractured by this stage and one in the bent-back frontal region close to the cloud head. It was shown in Figs. 9(e) and (f) that considerable potential for MSI existed in the bent-back front of the system at both 950
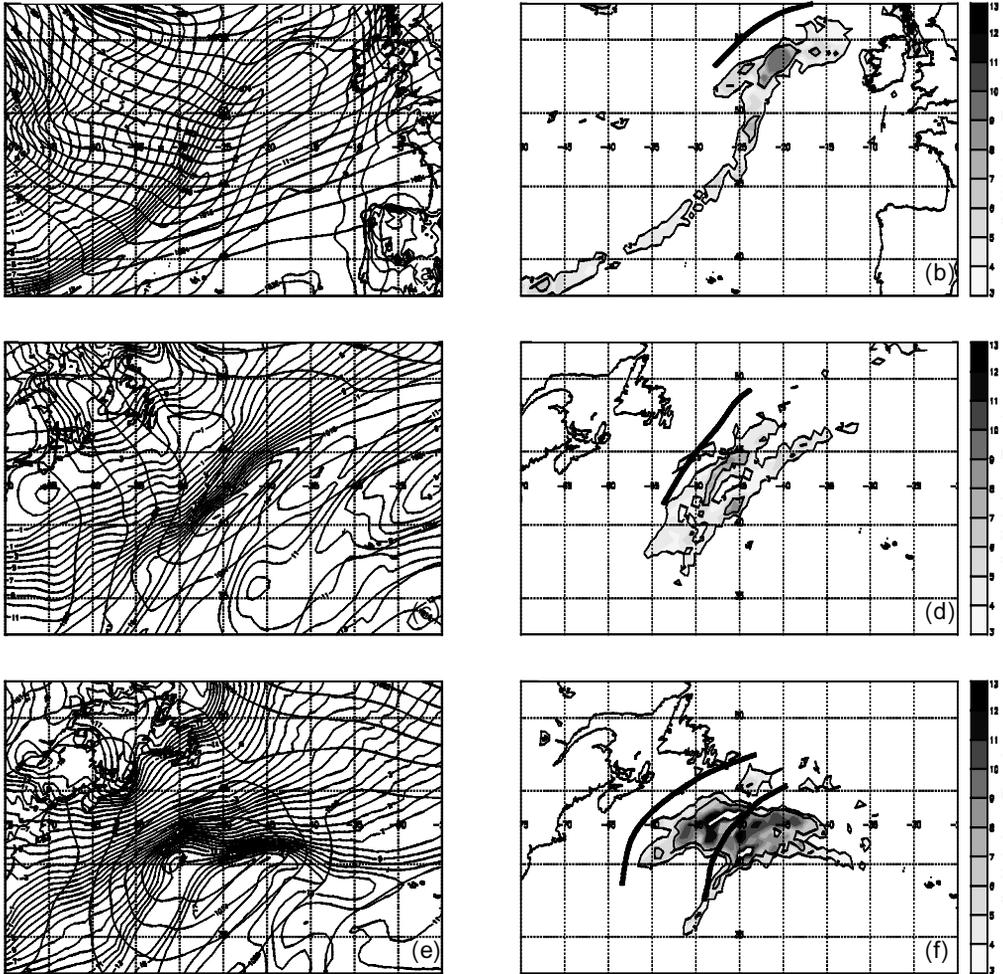
Figure 10.   Diagnostic of the vertically integrated extent of realizable symmetric instability (VRS, right-hand plots) and 950 mb wet-bulb potential temperature (°C) and sea-level pressure (mb) (left-hand plots) for three examples of weakly convex cloud heads. Scale on right-hand plots shows the number of vertical levels where conditions for the VRS diagnostic are met at each grid point. Thick black lines depict the cold-air boundaries of the cloud heads derived from satellite imagery. (a) and (b), 0600 UTC 17 February 1997. (c) and (d), 0000 UTC, 26 March 1998. (e) and (f), 0000 UTC, 18 February 1997.

and 750 mb. The VRS diagnostic in Fig. 11(b) backs up the SCAPE plots in suggesting a deep layer of actual MSI in this region.

This section has shown, using SCAPE and the VRS diagnostic, that there is abundant MSI in the frontal zones close to both weakly and strongly convex cloud heads. The introduction of the VRS diagnostic highlights regions where MSI is realizable rather than those with merely the potential for MSI, as shown by the SCAPE diagnostic. The VRS diagnostic points to realizable MSI in depth in the region along the cold-anafrontal zone that produces the CH_W. In the more mature systems associated with the CH_S, realizable MSI occurs in depth not only along the bent-back front but also along the trailing cold front.
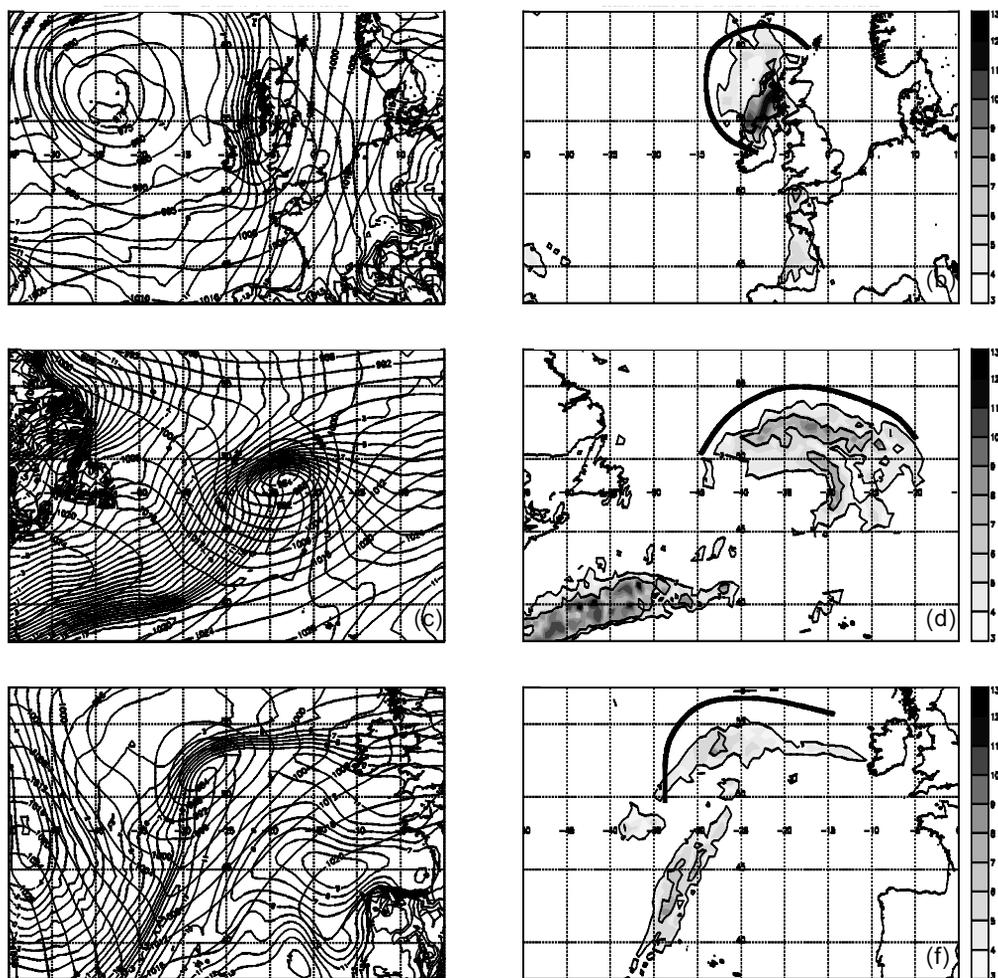
Figure 11. Diagnostic of the vertically integrated extent of realizable symmetric instability (VRS, right-hand plots) and 950 mb wet-bulb potential temperature (°C) and sea-level pressure (mb) (left-hand plots) for three examples of strongly convex cloud heads. Scale on right-hand plots shows the number of vertical levels where conditions for the VRS diagnostic are met at each grid point. Thick black lines depict the cold-air boundaries of the cloud heads. (a) and (b), 1800 UTC, 24 October 1995. (c) and (d), 1800 UTC, 25 December 1998. (e) and (f), 2100 UTC, 26 March 1998.

4. DISCUSSION AND CONCLUSIONS

The frontal regions analysed in this paper were all developing and were probably frontogenetic and so the response to frontogenetic forcing may have been enhanced by the presence of MSI. Emanuel (1985) and Thorpe and Emanuel (1985) first showed that with decreasing symmetric stability, the ascent at and ahead of the surface front would become more intense and localized. This argument was extended in viscous studies by Xu (1992) who showed that in the presence of MSI and weak frontal forcing, the updraught is further intensified and also may contain substructure in the form of smaller bands. Our results support the idea that enhanced frontal ascent may occur in the cloud-head regions that have been shown to be unstable to MSI. Specifically, we envisage that the net upward mass flux in frontal ascent might contain a component due to slantwise instability such that the total mass flux would exceed that required

to maintain geostrophic and hydrostatic balance (i.e. that which is under geostrophic control). This in turn implies enhanced rainfall totals.

Studies have shown (e.g. Lindstrom and Nordeng 1992; Persson and Warner 1993; Dixon 2000) that in the presence of MSI, NWP models need high resolution if the more intense aspects of the synoptic situation are to be sufficiently resolved. In previous studies, it has also been shown that NWP models that are unable to release MSI have underestimated the accumulated rainfall in frontal situations that appear symmetrically unstable. Lindstrom and Nordeng (1992) introduced slantwise convective parametrization in a study of a frontal situation that produced high rainfall amounts which had been significantly underestimated by the model prior to the introduction of the parametrization; they achieved significant improvement in the accumulated rainfall amounts. In the case of the LAM used in the present study, with its 50 km grid spacing and a low-to-middle tropospheric grid spacing of 500 m to 1 km, it is possible that the rainfall accumulations produced by its large-scale precipitation schemes are underestimated in synoptic situations where the atmosphere is moist slantwise-unstable in depth, as in the above examples. It may be that the new VRS diagnostic could be used as an early warning of frontal situations where rainfall may be underpredicted by coarse-gridded models. A benefit of the VRS diagnostic is that it highlights the depth of MSI in the atmosphere as opposed to the single-level estimate of MSI given by SCAPE. Moreover, SCAPE is a measure of only the *potential* for MSI and, as highlighted by Figs. 8(e) and (f), SCAPE may be large and exist in depth, but conditions for release of MSI (given by the VRS diagnostic in Fig. 10(b)) may only exist at a few levels. In addition, the speed of calculation of the VRS diagnostic when compared with a SCAPE calculation makes it more amenable if required by a forecaster. The speed arises partly from avoiding the computation of absolute-momentum surfaces and their orientation in the vertical. It could be argued, however, that the VRS diagnostic should similarly be computed in the direction of the local geostrophic vorticity vector rather than in the vertical.

It should be noted here that, given the underlying theory of MSI, the SCAPE and VRS diagnostics are relevant to regions that are two dimensional. This is often true of trailing cold fronts, for example those shown in Fig. 11, but the bent-back frontal regions associated with cloud heads exhibit more curvature, especially in the case of a CH_S, making this theory somewhat less applicable. Some MSI theory has been developed for curved flows (e.g. Sanders 1986) that may be more relevant to the bent-back frontal regions, but this is not considered here. Indeed, Gray and Thorpe (2001) have shown recently that in these highly three-dimensional situations, values of SCAPE that assume two dimensionality of flow may be greatly in error.

A life-cycle model for a cloud-head-bearing depression can be devised on the basis of the examples that were studied here. The sequence of events in Fig. 12 is a form of synthesis of the development of cyclones that possess cloud heads. The sequence that we have studied is idealized, although several cloud-head-bearing cyclone life cycles can be related well to this schematic of development. The thin arrows in the diagram highlight the direction of release of symmetric instability.

Stage 1: Initial cloud-head development. The initial development of the cloud head is often seen in the imagery as a region of lower cloud tops emerging from beneath the polar-front cloud band. This is the 'weakly convex cloud head' (CH_W) stage as defined earlier. However, as in the example from December 1997 in this paper, the PFCB does not always shield the developing cloud head. Our work suggests that the CH_W is due to cold-anafrontal circulations that may be

STAGE 1 - WEAKLY CONVEX CLOUD HEAD

STAGE 2 - TRANSITIONAL STAGE

STAGE 3 - STRONGLY CONVEX CLOUD HEAD

Cloud head/hook

SCAPE region at 950mb
and direction of realisation

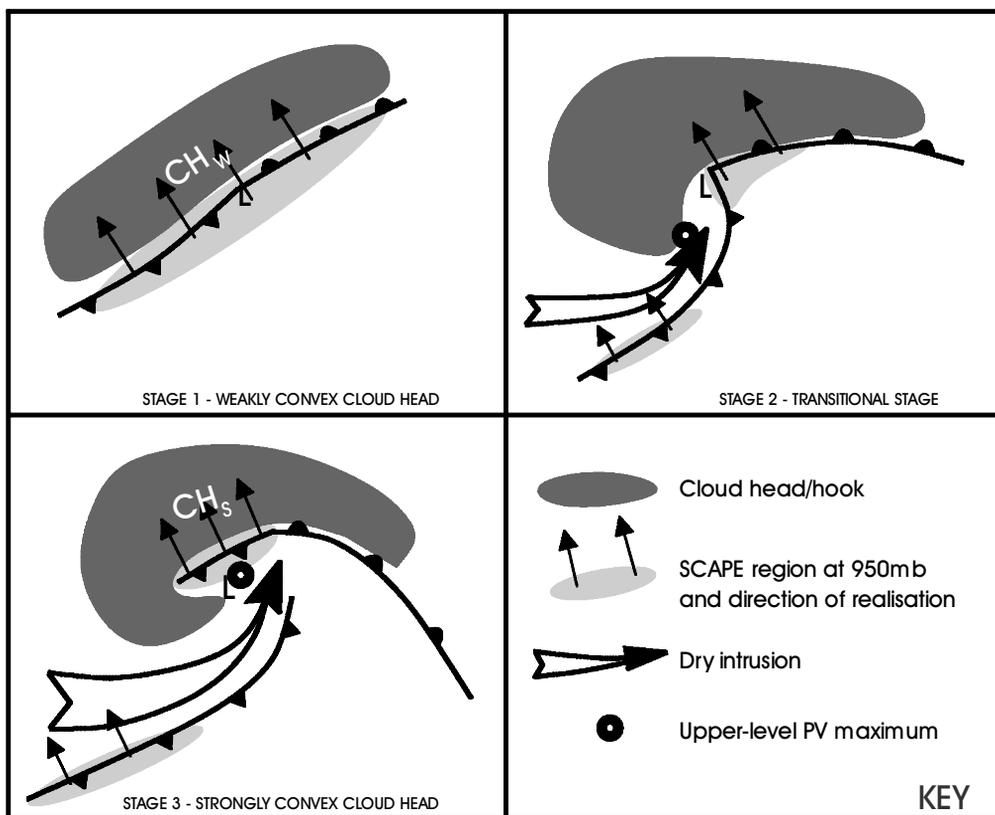Dry intrusion

Upper-level PV maximum

KEY

Figure 12.   Idealized cloud-head cyclone evolution based upon cyclones examined in the study.

invigorated by the presence of MSI. As discussed previously, these circulations may not be sufficiently resolved by coarse-gridded NWP models. The MSI is most intense and vertically extensive along the strongest thermal gradient, and it may be accompanied by low-level convective instability. Low-to-middle levels tend to have only MSI present.

Stage 2: Evidence of vorticity. After the initial formation of the cloud head, its outer edge often becomes more strongly convex. This is evidence that the low-level and/or upper-level vorticity feature is beginning to affect the CH_W. It is not known whether the low-level flow acts to bring down the tropopause and thus the two features interact or vice versa. Often the cloud head is seen to hook slightly at its westernmost point (assuming a thermal gradient lying west to east). MSI still exists in the warm sector of the cyclone, and later in this phase, MSI appears along the trailing cold front of the system. This is still prior to rapid deepening of the system. The surface thermal wave now shows greater signs of becoming wound up by the advective effects of the flow due to the upper-level PV anomaly. There is also evidence of the development of a dry intrusion.

Stage 3: Development of bent-back front and rapid deepening. At the later stages of development, usually when the system starts to develop rapidly, a bent-back front is formed to the north-west (in the northern hemisphere) of the developing low,

and the main cold front fractures from the warm front. The cloud head becomes strongly convex (CH_S) and very hooked, and it begins to form a spiral as part of it wraps around the low. Large SCAPE is found in a small region associated with the tight gradients and strong vertical wind shear in the region of the bent-back front. This potential for MSI appears to exist in great depth. The presence of this MSI may lead to underpredicted rainfall amounts in coarse-gridded models that are incapable of representing its release. There is also MSI in the trailing cold-frontal region, and this region may exist over a significant distance along the trailing cold front. The MSI may be much less prominent in the cold-frontal regions toward the centre of the low where the overrunning dry air leads to a cold katafront.

The ideas in this paper are qualitative in nature. It is to be hoped that they will stimulate others to follow up with quantitative confirmation of the interpretations.

REFERENCES

Bader, M. J., Forbes, G. S., Grant, J. R., Lilley, R. B. E. and Waters, A. J.	1995	*Images in Weather Forecasting*. Cambridge University Press
Bennetts, D. A. and Hoskins, B. J.	1979	Conditional symmetric instability—a possible explanation for frontal rainbands. *Q. J. R. Meteorol. Soc.*, **105**, 945–962
Böttger, H., Eckhardt, M. and Katergiannakis, U.	1975	Forecasting extratropical storms with hurricane intensity using satellite information. *J. Appl. Meteorol.*, **14**, 1259–1265
Browning, K. A. and Roberts, N. M.	1994	Structure of a frontal cyclone. *Q. J. R. Meteorol. Soc.*, **120**, 1535–1557
Browning, K. A., Ballard, S. P. and Davitt, C. S. A.	1997	High-resolution analysis of frontal fracture. *Mon. Weather Rev.*, **125**, 1212–1230
Carr, F. H. and Millard, J. P.	1985	A composite study of comma clouds and their association with severe weather over the Great Plains. *Mon. Weather Rev.*, **113**, 370–387
Cullen, M. J. P.	1993	The unified forecast climate model. *Meteorol. Mag.*, **122**, 81–94
DeVoir, G. A.	1998	'Conditional symmetric instability—methods of operational diagnosis and case study of 23–24 February 1994 eastern Washington/Oregon snowstorm'. National Weather Service Western Region Technical Memorandum, **254**
Dixon, R. S.	2000	'Diagnostic studies of symmetric instability'. PhD thesis, University of Reading
Doswell III, C. A., Brooks, E. and Maddox, R. A.	1996	Flash flood forecasting: An ingredients-based methodology. *Weather and Forecasting*, **11**, 560–581
Doty, K. G. and Perkey, D. J.	1993	Sensitivity of trajectory calculations to the temporal frequency of wind data. *Mon. Weather Rev.*, **121**, 387–401
Eliassen, A. and Kleinschmidt, E.	1957	Dynamic meteorology. Pp. 112–129 in *Handbuch der Physik*. Springer-Verlag, Berlin, Germany
Emanuel, K. A.	1983	On assessing local conditional symmetric instability from atmospheric soundings. *Mon. Weather Rev.*, **111**, 2016–2033
	1985	Frontal circulations in the presence of small moist symmetric stability. *J. Atmos. Sci.*, **42**, 1062–1071

Emanuel, K. A., Fantini, M. and Thorpe, A. — 1987 — Baroclinic instability in an environment of small stability to moist convection. Part 1: Two-dimensional models. *J. Atmos. Sci.*, **44,** 1559–1573

Gray, S. L. and Thorpe, A. J. — 2001 — Parcel theory in three-dimensions and the calculation of SCAPE. *Mon. Weather Rev.*, **129,** 1656–1672

Griffiths, M., Thorpe, A. J. and Browning, K. A. — 2000 — Convective destabilization by a tropopause fold diagnosed using potential vorticity inversion. *Q. J. R. Meteorol. Soc.*, **126,** 125–144

Hoskins, B. J. — 1974 — The role of potential vorticity in symmetric stability and instability. *Q. J. R. Meteorol. Soc.*, **100,** 480–482

Hoskins, B. J., McIntyre, M. E. and Robertson, A. W. — 1985 — On the use and significance of isentropic potential vorticity maps. *Q. J. R. Meteorol. Soc.*, **111,** 877–946

Lindstrom, S. S. and Nordeng, T. E. — 1992 — Parameterised slantwise convection in a numerical model. *Mon. Weather Rev.*, **120,** 742–756

Lussky, G. R. — 1989 — Heavy rains and flooding in Montana: A case for operational use of symmetric instability diagnosis. *Weather and Forecasting*, **4,** 186–201

McCallum, E. and Norris, W. J. T. — 1990 — The storms of January and February 1990. *Meteorol. Mag.*, **119,** 201–210

McNulty, R. P. — 1995 — Severe convective weather: A central region forecasting challenge. *Weather and Forecasting*, **10,** 187–202

Monk, G. A. and Bader, M. J. — 1988 — Satellite images of development of the storm. *Weather*, **43,** 130–136

Moore, J. T. and Blakley, P. D. — 1988 — The role of frontogenetical forcing and conditional symmetric instability in the midwest snowstorm of 30–31 January 1982. *Mon. Weather Rev.*, **116,** 2155–2171

Persson, P. O. G. and Warner, T. T. — 1993 — Nonlinear hydrostatic conditional symmetric instability: Implications for numerical weather prediction. *Mon. Weather Rev.*, **121,** 1821–1833

Sanders, F. — 1986 — Frontogenesis and symmetric stability in a major New England snowstorm. *Mon. Weather Rev.*, **114,** 1847–1862

Schultz, D. M. and Schumacher, P. N. — 1999 — The use and misuse of conditional symmetric instability. *Mon. Weather Rev.*, **127,** 2709–2732

Shapiro, M. A. and Keyser, D. — 1990 — Fronts, jet streams and the tropopause. Pp. 167–191 in *Extra-tropical cyclones: The Erik Palmen memorial volume, C.* Eds. W. Newton and E. O. Holopainen, Am. Meteorol. Soc.

Shutts, G. J. — 1990a — Dynamical aspects of the October storm 1987: A study of a successful fine mesh simulation. *Q. J. R. Meteorol. Soc.*, **116,** 1315–1347

— 1990b — SCAPE charts from numerical weather prediction fields. *Mon. Weather Rev.*, **118,** 2745–2751

Thorpe, A. J. and Emanuel, K. A. — 1985 — Frontogenesis in the presence of small stability to slantwise convection. *J. Atmos. Sci.*, **42,** 1809–1824

Wernli, H. — 1997 — Lagrangian-based analysis of extra-tropical cyclones. 1: The method and its applications. *Q. J. R. Meteorol. Soc.*, **123,** 467–489

Xu, Q. — 1992 — Frontal circulations in the presence of small viscous moist symmetric stability and weak forcing. *Q. J. R. Meteorol. Soc.*, **115,** 1325–1353

Young, M. V., Monk, G. A. and Browning, K. A. — 1987 — Interpretation of satellite imagery of a rapidly deepening cyclone. *Q. J. R. Meteorol. Soc.*, **113,** 1089–1100